JCTC Journal of Chemical Theory and Computation

ARTICLE

pubs.acs.org/JCTC

Linear Scaling Hierarchical Integration Scheme for the Exchange-Correlation Term in Molecular and Periodic Systems

Asbjörn M. Burow and Marek Sierka*

Institut für Chemie, Humboldt-Universität zu Berlin, Unter den Linden 6, D-10099 Berlin, Germany

Supporting Information

ABSTRACT: An adaptive numerical integration scheme for efficient evaluation of the exchange-correlation term using localized basis functions and atom-centered grids is presented. The method treats molecules and systems with periodic boundary conditions on an equal footing. Its computational efficiency and $O(N)$ scaling with the system size is achieved by a hierarchical spatial grouping of basis functions and grid points using an octree. This allows for an efficient screening of negligible contributions and an optimal use of hardware-optimized matrix−matrix multiplication subroutines, such as BLAS. The implementation of the method within the TURBOMOLE program package demonstrates consistent accuracy and efficiency across molecular and periodic systems.

1. INTRODUCTION

Density functional theory (DFT) is distinguished from traditional wave function based *ab initio* methods by its treatment of the exchange-correlation contributions to the total energy as one-electron integrals, notwithstanding the fact that they originate from many-electron interactions. These one-electron integrals contain the exchange-correlation function[1−9] $f(\mathbf{r})$ and are invariably too complex to permit their evaluation in analytical form. Consequently, the function $f(\mathbf{r})$ is integrated numerically on a finite set of grid points $\mathbf{r}_m$, i.e.,

$$\int f(\mathbf{r})\,\mathrm{d}\mathbf{r} = \sum_m w_m \times f(\mathbf{r}_m) \tag{1}$$

with weights w_m depending on the grid point distribution. The strongly peaked nature of function f about nuclear centers requires special treatment and has inspired sophisticated algorithms, yielding numerical integration schemes with an optimum number of grid points per atom. There are different methodologies for the numerical evaluation implemented in various programs, such as DMOL,[10] GAUSSIAN,[11] CRYSTAL,[12] ADF,[13] MONDOSCF,[14] deMon2k,[15] Q-Chem,[16] ORCA,[17] and FHI-aims.[18] For DFT calculations employing plane wave basis sets, uniformly spaced Cartesian grids are mainly used since they significantly simplify the fast Fourier transform. However, due to the strong variations of $f(\mathbf{r})$, these grids require special modification, e.g., the use of curvilinear coordinates,[19−21] in order to obtain high accuracy. In addition, for DFT calculations using local basis sets, there are other ways to obtain grids adapted to the strongly peaked regions of $f(\mathbf{r})$ in polyatomic systems, e.g., hierarchical Cartesian grids[14] and multicenter grids. The multicenter grids are composed of atom-centered grids and are restricted to the atoms of the unit cell (UC) in the case of periodic systems. The grid points of each atom-centered grid are usually arranged in Lebedev spheres[22−24] of several radii.[25−29] For such multicenter grids, several schemes[10,11,30−36] are available to calculate the weights w_m of grid points $\mathbf{r}_m$ belonging to the atoms i. A technique often applied is the renormalization of atomic weights w_m^{at} using the continuous partition function $P_i(\mathbf{r})$, i.e.,

$$w_m = P_i(\mathbf{r}_m) \times w_m^{\mathrm{at}} \tag{2}$$

There are several schemes to compute this partition function using, e.g., spherical atomic electron densities[10,35] or purely geometric considerations.[11,34] The atomic weights w_m^{at}, i.e., the weights of isolated atoms, are usually determined using radial and spherical quadrature schemes.[24−29,37]

For the multicenter grids, a highly efficient evaluation of the exchange-correlation term is achieved using hardware-optimized matrix−matrix multiplication subroutines, such as basic linear algebra subprograms (BLAS).[38,39] For this, the necessary matrices are constructed by grouping grid points and basis functions into batches. Using local basis functions and prescreening techniques, each matrix contains exclusively the basis functions which have non-negligible contributions to the corresponding grid points. The multiplication of these matrices with blocks of the density matrix is required for the computation of the electron density and its gradients on the grid. For efficient use of the matrix−matrix multiplication subroutines, the dimensions of the matrices, i.e., the number of grid points and basis functions in the batches, should be as large as possible. However, local basis functions have non-negligible contributions only to a limited number of grid points. Therefore, the optimum choice of batch sizes has to balance the computational gain due to the efficiency of the matrix−matrix multiplications and the computational loss due to zero entries in the matrices caused by the local character of the basis functions. Although the use of batches is mentioned in several works,[17,28,40−42] there are only a few that discuss batch shapes[11] and the use of hierarchical batching schemes.[14,43] Hierarchical batching ideas were also used to add the exact and screened Fock exchange pieces in DFT.[44]

Here, we present a new hierarchical scheme for efficient numerical evaluation of the exchange-correlation term within

Received: June 17, 2011
Published: August 08, 2011

orbital-based DFT employing localized basis functions. The method treats molecular and periodic systems of any dimensionality on an equal footing. It uses grid point batches of different sizes which overlap in space so that optimal batch sizes can be selected for different spatial extents of the basis functions. This is facilitated by grouping the grid points in batches belonging to the domains of an octree. Similar hierarchical structures are employed, e.g., for evaluation of the Coulomb term using the fast multipole method.[45,46] This way, our present hierarchical numerical integration algorithm efficiently uses a multilevel batch approach combined with hardware-optimized matrix−matrix multiplications. Its implementation within the TURBOMOLE program package[47,48] shows linear scaling with an increasing number of basis functions for a variety of molecular and periodic systems.

2. METHOD

2.1. Kohn−Sham Equations. In the orbital-based DFT under periodic boundary conditions (PBC), the canonical orbital coefficients matrix $\mathbf{C}^{\mathbf{k}}$ at each reciprocal lattice point $\mathbf{k}$ satisfies

$$\mathbf{F}^{\mathbf{k}}\mathbf{C}^{\mathbf{k}} = \mathbf{S}^{\mathbf{k}}\mathbf{C}^{\mathbf{k}}\boldsymbol{\varepsilon}^{\mathbf{k}} \tag{3}$$

with the Fock matrix $\mathbf{F}^{\mathbf{k}}$, the overlap matrix $\mathbf{S}^{\mathbf{k}}$, and the diagonal matrix $\boldsymbol{\varepsilon}^{\mathbf{k}}$ of orbital energies. The elements $c^{\mathbf{k}}_{\mu l}$ of the matrix $\mathbf{C}^{\mathbf{k}}$ belong to the orbitals

$$\psi^{\mathbf{k}}_{l} = \sum_{\mu} c^{\mathbf{k}}_{\mu l}\phi^{\mathbf{k}}_{\mu} \tag{4}$$

constructed from periodic Bloch functions

$$\phi^{\mathbf{k}}_{\mu} = \sum_{\mathbf{L}} e^{i\mathbf{k}\mathbf{L}}\xi^{\mathbf{L}}_{\mu} \tag{5}$$

with local basis functions $\xi^{\mathbf{L}}_{\mu}$ centered at positions $\mathbf{R}_{\mu} + \mathbf{L}$, where $\mathbf{R}_{\mu}$ are the positions of the atoms in the UC and $\mathbf{L}$ are the lattice vectors in direct space. The basis functions $\xi^{\mathbf{L}}_{\mu}$ are represented as linear combinations

$$\xi^{\mathbf{L}}_{\mu}(\mathbf{r}) = \sum_{\kappa=1}^{n_{\mu}} d_{\mu\kappa}\varphi^{\mathbf{L}}_{\mu\kappa}(\mathbf{r}) \tag{6}$$

of a small number n_{μ} of primitive Cartesian Gaussian-type functions (CGTF) $\varphi^{\mathbf{L}}_{\mu\kappa}$. The CGTF are defined as

$$\varphi^{\mathbf{L}}_{\mu\kappa}(\mathbf{r}) = (x - R_{\mu x})^{\prime_x}(y - R_{\mu y})^{\prime_y}(z - R_{\mu z})^{\prime_z} \times \exp(-\zeta_{\mu\kappa}|\mathbf{r} - \mathbf{R}_{\mu} - \mathbf{L}|^2) \tag{7}$$

with the Cartesian components x, y, and z of $\mathbf{r}$. The real exponent $\zeta_{\mu\kappa}$ and the integer exponents $\prime_x$, $\prime_y$, and $\prime_z$ specify the radial and the angular parts of the function, respectively. Equations 3−7 hold also for the molecular case, where $\mathbf{k} = 0$ and $\mathbf{L} = 0$.

The Fock matrix $\mathbf{F}^{\mathbf{k}}$ is the sum of kinetic energy matrix $\mathbf{T}^{\mathbf{k}}$, Coulomb matrix $\mathbf{J}^{\mathbf{k}}$, and exchange-correlation matrix $\mathbf{X}^{\mathbf{k}}$. Using CGTF, the matrices $\mathbf{T}^{\mathbf{k}}$ and $\mathbf{J}^{\mathbf{k}}$ can be evaluated by analytical expressions, whereas the elements of $\mathbf{X}^{\mathbf{k}}$ are evaluated by numerical integration. The elements of the exchange-correlation matrix $\mathbf{X}^{\mathbf{k}}$ are defined as

$$X^{\mathbf{k}}_{\mu\nu} = \sum_{\mathbf{L}'} e^{i\mathbf{k}\mathbf{L}'} X^{\mathbf{L}'}_{\mu\nu} \text{ with } X^{\mathbf{L}'}_{\mu\nu} = \int \hat{O}_{\mathrm{XC}}[\xi^{0}_{\mu}\xi^{\mathbf{L}'}_{\nu}]\, \mathbf{dr} \tag{8}$$

where $X^{\mathbf{L}'}_{\mu\nu}$ ($\mathbf{L}' = 0$ for molecules) and $\hat{O}_{\mathrm{XC}}$ are the real space exchange-correlation matrix and the exchange-correlation operator, respectively. For closed shell systems in the generalized gradient approximation, the operator $\hat{O}_{\mathrm{XC}}$ is expressed as

$$\hat{O}_{\mathrm{XC}} = \frac{\partial f}{\partial \rho} + 2\frac{\partial f}{\partial(|\nabla\rho|^2)}\nabla\rho\nabla \tag{9}$$

in terms of the exchange-correlation function[1−9] $f(\rho(\mathbf{r}), |\nabla\rho(\mathbf{r})|^2)$ and the electron density ρ. The second term in eq 9 disappears in the local density approximation. For spin-dependent DFT in the unrestricted formalism, the form of $\hat{O}_{\mathrm{XC}}$ is presented elsewhere.[1,49] The integration of the exchange-correlation function over the UC yields the exchange-correlation energy

$$E_{\mathrm{XC}} = \int_{\mathrm{UC}} f(\rho(\mathbf{r}), |\nabla\rho(\mathbf{r})|^2)\, \mathbf{dr} \tag{10}$$

for both closed shell and spin-unrestricted cases. For molecules, the integration in eq 10 spans the entire space.

2.2. Quadrature on the Grid. The terms $X^{\mathbf{L}'}_{\mu\nu}$ and E_{XC} in eqs 8 and 10 are evaluated numerically on a set of grid points $\mathbf{r}_m$ belonging to the atoms i. The energy expression is given by

$$E_{\mathrm{XC}} = \sum_{i}\sum_{m\in i} w_m \times f(\rho^m, |\nabla\rho^m|^2) \tag{11}$$

with the weights w_m defined in eq 2 and with $\rho^m = \rho(\mathbf{r}_m)$. In periodic systems[50,51] and molecules, the summation runs over the atoms i of the UC and the whole molecule, respectively. The exchange-correlation matrix [eq 8] is evaluated numerically as

$$X^{\mathbf{L}'}_{\mu\nu} = \sum_{i}\sum_{m\in i} X^{\mathbf{L}',m}_{\mu\nu} \tag{12}$$

with contributions $X^{\mathbf{L}',m}_{\mu\nu}$ from the grid points $\mathbf{r}_m$ defined as

$$X^{\mathbf{L}',m}_{\mu\nu} = w_m \sum_{\mathbf{L}} \hat{O}_{\mathrm{XC}}[\xi^{\mathbf{L},m}_{\mu}\xi^{\mathbf{L}+\mathbf{L}',m}_{\nu}] \tag{13}$$

using weights w_m [eq 2]. Insertion of the closed shell form of the exchange-correlation operator $\hat{O}_{\mathrm{XC}}$ [eq 9] into eq 13 yields

$$X^{\mathbf{L}',m}_{\mu\nu} = \sum_{\mathbf{L}}(\xi^{\mathbf{L},m}_{\mu}z^{\mathbf{L}+\mathbf{L}',m}_{\nu} + z^{\mathbf{L},m}_{\mu}\xi^{\mathbf{L}+\mathbf{L}',m}_{\nu}) \tag{14}$$

with the potential

$$z^{\mathbf{L},m}_{\mu} = \frac{1}{2}F^m\xi^{\mathbf{L},m}_{\mu} + \sum_{\alpha} F^m_{\alpha}\xi^{\mathbf{L},m}_{\mu\alpha} \tag{15}$$

where $\xi^{\mathbf{L},m}_{\mu}$ and $\xi^{\mathbf{L},m}_{\mu\alpha} = \partial\xi^{\mathbf{L},m}_{\mu}/\partial\alpha$ ($\alpha = x, y, z$) denote values of the basis functions and their gradients, respectively, on the grid points $\mathbf{r}_m$. The terms F^m and F^m_{α} are defined as

$$F^m = w_m\left.\frac{\partial f}{\partial\rho}\right|_{\mathbf{r}_m} \tag{16}$$

$$(F^m_x, F^m_y, F^m_z) = 2w_m\left.\frac{\partial f}{\partial(|\nabla\rho|^2)}\nabla\rho\right|_{\mathbf{r}_m} \tag{17}$$

The molecular case is obtained setting $\mathbf{L} = 0$ and $\mathbf{L}' = 0$.

The computation of the exchange-correlation energy and the potential [eqs 11 and 15] requires evaluation of the electron density ρ and its gradient $\nabla\rho$ on the grid. The electron density ρ^m on the grid points $\mathbf{r}_m$ is defined as the linear combination of basis

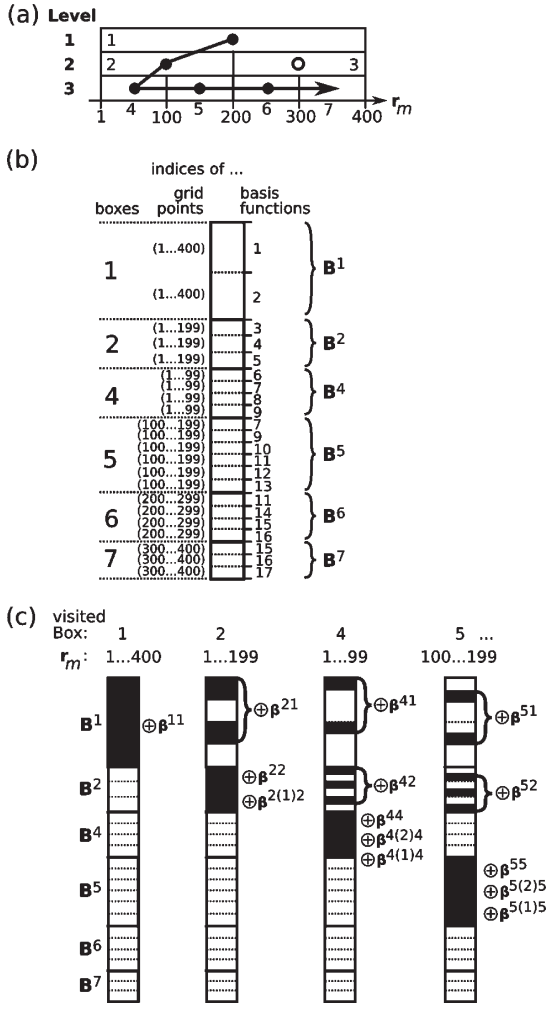

Figure 1. Example of the integration scheme. (a) Branch of boxes q in a binary tree (octree: eight children per parent box). Each box contains the grid points $\mathbf{r}_m$. Box 3 is empty. (b) One-dimensional array of matrices $\mathbf{B}^q$. Indices show grid points and basis functions assigned to boxes. (c) Accumulation ($\oplus$) of $\boldsymbol{\beta}^{pq}$ and $\boldsymbol{\beta}^{p(q)p}$ on $\mathbf{B}^q$ and $\mathbf{B}^p$ in loop 1 of Algorithm 1. For each visited box, the rectangle displays the array defined in b, where black areas highlight the changed content on the grid points $\mathbf{r}_m$.

function products

$$\rho^m = \sum_{\mu\mathbf{L}}\sum_{\nu\mathbf{L}'} D_{\mu\nu}^{\mathbf{L}'-\mathbf{L}}\xi_\mu^{\mathbf{L},m}\xi_\nu^{\mathbf{L}',m} \tag{18}$$

with the real space density matrix elements[52] $D_{\mu\nu}^{\mathbf{L}'-\mathbf{L}}$ ($\mathbf{L} = 0$ and $\mathbf{L}' = 0$ for molecules). The partial derivatives of ρ with respect to the Cartesian coordinates $\alpha = x, y, z$ yield the components ρ_α of the gradient $\nabla\rho$, i.e.,

$$\rho_\alpha^m = \left.\frac{\partial\rho}{\partial\alpha}\right|_{\mathbf{r}_m} = \sum_{\mu\mathbf{L}}\sum_{\nu\mathbf{L}'} D_{\mu\nu}^{\mathbf{L}'-\mathbf{L}}(\xi_{\mu\alpha}^{\mathbf{L},m}\xi_\nu^{\mathbf{L}',m} + \xi_\mu^{\mathbf{L},m}\xi_{\nu\alpha}^{\mathbf{L}',m}) \tag{19}$$

Since a limited number of local basis functions contributes to each grid point, the computational effort per grid point remains constant and the evaluation of the exchange-correlation term scales linearly with the system size (number of grid points).

2.3. Grouping Grid Points and Basis Functions. An efficient numerical computation of the electron density [eq 18] and the gradients [eq 19] on the grid is achieved using optimized matrix−matrix multiplication subroutines. For this, the necessary matrices are constructed by grouping grid points and basis functions using an octree. First, a cubic box enclosing all grid points is defined as the parent box of the octree. This parent box is bisected along each Cartesian axis to yield a set of eight child boxes belonging to the next lower level. Each of these child boxes is subdivided, creating children of the children, like the generations of a computational family tree. The number of divisions is chosen to yield box sizes optimal for the performance of the numerical integration. In the next step, all grid points and basis functions are sorted into the octree. Grid points are sorted into the boxes of the tree by coordinates. The sorting of basis functions into boxes is based on their spatial extents.[11,53] For this, spheres of the radii[53]

$$r_\mu = \max_\kappa\left(\sqrt{\frac{-\ln\varepsilon + 0.5\times\ln\zeta_{\mu\kappa}}{\zeta_{\mu\kappa}}}\right) \tag{20}$$

centered at the atomic positions $\mathbf{R}_\mu + \mathbf{L}$ are assigned to the basis functions $\xi_\mu^{\mathbf{L}}$ [eq 6], where ε is a precision parameter. Starting from the highest level, each basis function is assigned to the boxes at a given level which are fully enclosed by the corresponding sphere. If the basis function is assigned to a box, then its child boxes at the following levels are removed from the assignment for this function. Occupied boxes contain at least one grid point and one basis function. Root boxes are occupied boxes without any occupied parent at higher levels. A branch is formed by a root box and its occupied child boxes. The boxes p of a branch are ordered by levels from top to bottom (see Figure 1).

2.4. Exchange-Correlation Term in the Octree. This section describes the evaluation of the exchange-correlation term in the octree. First, the necessary terms and notations are defined. For each box p of the octree, the values of basis functions on the grid, $\xi_\mu^{\mathbf{L},m}$, are arranged in a rectangular $M_p \times K_p$ matrix $\boldsymbol{\xi}^p$ (i.e., a batch), where M_p and K_p are the number of grid points and the number of basis functions, respectively. Similarly, $\boldsymbol{\xi}_\alpha^p$ denotes the matrices containing gradients of basis functions on the grid points in the box p. The $M_p \times K_q$ matrices $\boldsymbol{\xi}^{p(q)}$ contain the values of the basis functions, $\xi_\mu^{\mathbf{L},m}$, assigned to a parent box q, on the grid points of its child box p. The $K_p \times K_q$ matrices $\mathbf{D}^{pq}$ denote submatrices of the density matrix. They are formed from the elements $D_{\mu\nu}^{\mathbf{L}'-\mathbf{L}}$ belonging to the functions $\xi_\mu^{\mathbf{L}}$ and $\xi_\nu^{\mathbf{L}'}$, assigned to the boxes p and q, respectively. The $M_q \times K_q$ matrices $\mathbf{B}^q$ defined for each box q are used to accumulate the $M_p \times K_q$ matrices

$$\boldsymbol{\beta}^{pq} = \boldsymbol{\xi}^p\mathbf{D}^{pq} \tag{21}$$

calculated for child boxes p. This accumulation is denoted as

$$\mathbf{B}^q \leftarrow \mathbf{B}^q \oplus \boldsymbol{\beta}^{pq} \tag{22}$$

The columns of the matrices $\mathbf{B}^q$ and $\boldsymbol{\beta}^{pq}$ correspond to the same set of K_q basis functions. The rows of $\mathbf{B}^q$ correspond to M_q grid points in a box q, and the rows of $\boldsymbol{\beta}^{pq}$ correspond to M_p grid points of a child box p. The mth row of a matrix $\mathbf{M}$ is denoted as $\mathrm{row}_m[\mathbf{M}]$. Using these definitions, Algorithm 1 shows the computation of the electron density ρ and its gradients ρ_α on the grid for a single branch of the octree. The electron density and its gradients in different branches are independent of each other.

Algorithm 1. Compute Electron Density and Gradients within a Single Branch

(1) For each box p of the branch:
(2) Initialize $\mathbf{B}^p$ to zero
(3) Compute and save: $\boldsymbol{\xi}^p$ and $\boldsymbol{\xi}^p_\alpha$
(4) For each box q with $q = (p$ and all parent boxes of $p)$:
(5) Form $\mathbf{D}^{pq}$
(6) $\boldsymbol{\beta}^{pq} = \boldsymbol{\xi}^p \mathbf{D}^{pq}$
(7) $\mathbf{B}^q \leftarrow \mathbf{B}^q \oplus \boldsymbol{\beta}^{pq}$
(8) If $q \neq p$:
(9) $\boldsymbol{\beta}^{p(q)p} = \boldsymbol{\xi}^{p(q)} (\mathbf{D}^{pq})^{\mathrm{T}}$
(10) $\mathbf{B}^p \leftarrow \mathbf{B}^p \oplus \boldsymbol{\beta}^{p(q)p}$
(11) Initialize ρ and ρ_α to zero
(12) For each box p of the branch:
(13) For each $\mathbf{r}_m$ in p:
(14) $\rho^m \leftarrow \rho^m + \mathrm{row}_m[\mathbf{B}^p] \times \mathrm{row}_m[\boldsymbol{\xi}^p]^{\mathrm{T}}$
(15) $\rho_\alpha{}^m \leftarrow \rho_\alpha^m + 2 \times \mathrm{row}_m[\mathbf{B}^p] \times \mathrm{row}_m[\boldsymbol{\xi}^p_\alpha]^{\mathrm{T}}$

Figure 1 shows an example for the storage of the matrices $\mathbf{B}^p$ of a branch as a one-dimensional array and the accumulation of the matrices $\boldsymbol{\beta}^{pq}$ and $\boldsymbol{\beta}^{p(q)p}$ in steps 7 and 10 of Algorithm 1. The values of the electron density and the gradients on the grid obtained with Algorithm 1 are used in the Algorithm 2, which describes the numerical integration for the exchange-correlation energy E_{XC} [eq 11] and the matrix elements $X^{\mathbf{L}'}_{\mu\nu}$ [eq 12].

Algorithm 2. Compute E_{XC} and Matrix Elements $\mathbf{X}^{\mathbf{L}'}_{\mu\nu}$

(1) For each branch:
(2) Perform Algorithm 1 (compute and save: $\boldsymbol{\xi}^p, \boldsymbol{\xi}^p_\alpha, \rho, \rho_\alpha$)
(3) {For each $\mathbf{r}_m$ in the root box:
(4) $E_{\mathrm{XC}} \leftarrow E_{\mathrm{XC}} + w_m \times f(\rho^m, |\nabla\rho^m|^2)$
(5) Compute and save: F^m, F^m_x, F^m_y, F^m_z}
(6) For each box p of the branch:
(7) {For each $\xi^{\mathbf{L}}_\mu$ and $\mathbf{r}_m$ in p:
(8) Compute and save: $z^{\mathbf{L},m}_\mu$}
(9) For each box q with $q = (p$ and all parent boxes of $p)$:
(10) For each $\xi^{\mathbf{L}}_\mu$ in p and $\xi^{\mathbf{L}'}_\nu$ in q:
(11) For each $\mathbf{r}_m$ in p:
(12) $X^{\mathbf{L}'-\mathbf{L}}_{\mu\nu} \leftarrow X^{\mathbf{L}'-\mathbf{L}}_{\mu\nu} + \xi^{\mathbf{L},m}_\mu z^{\mathbf{L}',m}_\nu + z^{\mathbf{L},m}_\mu \xi^{\mathbf{L}',m}_\nu$
(13) If $q \neq p$: $X^{\mathbf{L}-\mathbf{L}'}_{\nu\mu} \leftarrow X^{\mathbf{L}-\mathbf{L}'}_{\nu\mu} + \xi^{\mathbf{L}',m}_\nu z^{\mathbf{L},m}_\mu + z^{\mathbf{L}',m}_\nu \xi^{\mathbf{L},m}_\mu$

Our implementation uses the symmetry

$$X^{\mathbf{L}'-\mathbf{L}}_{\mu\nu} = X^{\mathbf{L}-\mathbf{L}'}_{\nu\mu} \tag{23}$$

in steps 12 and 13 of Algorithm 2. The computational demand of steps 2, 3, and 6 of Algorithm 2 is independent of the system size, while the number of branches scales with $O(N)$. The computational efficiency is achieved using optimized matrix−matrix multiplications for products between the matrices $\boldsymbol{\xi}$ and $\mathbf{D}$ in steps 6 and 9 of Algorithm 1. This becomes so efficient that the evaluation of the matrix elements in steps 12 and 13 of Algorithm 2 can be the bottleneck of the calculation. Therefore, a two-level screening procedure is applied for efficient evaluation of elements $X^{\mathbf{L}'-\mathbf{L}}_{\mu\nu}$. First, an upper bound $X^{\max(pq)}$ of the contributions $X^{\mathbf{L}'-\mathbf{L},m}_{\mu\nu}$ from each pair of boxes p, q is determined within loop 9 of Algorithm 2 with

$$X^{\max(pq)} = \xi^{\max(p)} z^{\max(q)} + z^{\max(p)} \xi^{\max(q)} \tag{24}$$

employing the maximum values of basis functions, $\xi^{\max(s)}$, and potentials, $z^{\max(s)}$, in the boxes $s = p$, q,

Table 1. Specifications of Grids[a]

		H, He		Li−Ne		Na−Ar	
grid	$n^{\mathrm{outer},b}_\omega$	n_{r}	n_{tot}	n_{r}	n_{tot}	n_{r}	n_{tot}
3	302	10/5/15	5340	11/6/18	6382	13/7/20	7148
5	590	18/9/28	17978	20/10/30	19320	21/11/33	21226
7	1202	28/14/43	53954	30/15/45	56520	31/16/48	60262

[a] Number of outer angular grid points, $n^{\mathrm{outer}}_\omega$; number of radial grid points, n_{r}, (splitted into $n^{\mathrm{inner}}_{\mathrm{r}}/n^{\mathrm{medium}}_{\mathrm{r}}/n^{\mathrm{outer}}_{\mathrm{r}}$); and total number of grid points per atom, n_{tot}. [b] The number of angular grid points in the inner and medium regions are always $n^{\mathrm{inner}}_\omega = 26$ and $n^{\mathrm{medium}}_\omega = 110$, respectively.

$$\xi^{\max(s)} = \max_{\{\mathbf{r}_m,\mu,\mathbf{L}\}\in s} (\xi^{\mathbf{L},m}_\mu) \tag{25}$$

$$z^{\max(s)} = \max_{\{\mathbf{r}_m,\mu,\mathbf{L}\}\in s} (z^{\mathbf{L},m}_\mu) \tag{26}$$

All contributions $X^{\mathbf{L}'-\mathbf{L},m}_{\mu\nu}$ from the pair of boxes p, q are neglected in steps 12 and 13 of Algorithm 2 if the upper bound $b = X^{\max(pq)}$ satisfies

$$b \times M_p < \tau \tag{27}$$

with a threshold parameter τ. Second, if eq 27 is not satisfied, then an upper bound $X^{\mathbf{L}'-\mathbf{L},\max(pq)}_{\mu\nu}$ of the contributions $X^{\mathbf{L}'-\mathbf{L},m}_{\mu\nu}$ from each pair of basis functions $\xi^{\mathbf{L}}_\mu$, $\xi^{\mathbf{L}'}_\nu$ within the boxes pair p, q is determined with

$$X^{\mathbf{L}'-\mathbf{L},\max(pq)}_{\mu\nu} = \xi^{\mathbf{L},\max(p)}_\mu z^{\mathbf{L}',\max(q)}_\nu + z^{\mathbf{L},\max(p)}_\mu \xi^{\mathbf{L}',\max(q)}_\nu \tag{28}$$

For this, the maximum values of basis functions and potentials for each pair μ, $\mathbf{L}$ in a box $s = p$, q are used:

$$\xi^{\mathbf{L},\max(s)}_\mu = \max_{\mathbf{r}_m\in s} (\xi^{\mathbf{L},m}_\mu) \tag{29}$$

$$z^{\mathbf{L},\max(s)}_\mu = \max_{\mathbf{r}_m\in s} (z^{\mathbf{L},m}_\mu) \tag{30}$$

If eq 27 is satisfied for $b = X^{\mathbf{L}'-\mathbf{L},\max(pq)}_{\mu\nu}$, then the contributions $X^{\mathbf{L}'-\mathbf{L},m}_{\mu\nu}$ of the corresponding pair of basis functions are neglected for the boxes pair p, q.

3. COMPUTATIONS

The numerical accuracy and the scaling of our method are investigated using several molecular and periodic systems. The errors in the calculated electron numbers and the convergence of exchange-correlation energies with increasing grid size are used as criteria for assessment of the numerical accuracy. Electron numbers and exchange-correlation energies are obtained by numerical integration using converged electron densities from self-consistent field (SCF) calculations with a convergence threshold of 1.0×10^{-10} hartree for total energy and exchange-correlation energy. The scaling of the numerical integration with respect to increasing system sizes is investigated measuring CPU timings for a single SCF step.

3.1. Computational Details. All calculations are performed using the B-LYP exchange-correlation functional[6,7] with double-, triple-, and quadruple-ζ valence split basis sets plus polarization

functions (DZVP,[54] TZVP,[55] and QZVP,[56] respectively) and standard grid sizes[28] 3, 5, and 7 of TURBOMOLE. The details of the integration grids are shown in Table 1. The total numbers of grid points per atom, n_{tot}, can be calculated as[28]

$$n_{tot} = \sum_{\alpha} n_{\omega}^{\alpha} \times n_{r}^{\alpha} \text{ with } \alpha = \text{inner, medium, outer} \quad (31)$$

with the numbers of angular (n_{ω}^{α}) and radial (n_{r}^{α}) grid points of each atomic grid region α. The n_{ω}^{α} angular points of each atom form the angular grid on a unit sphere. The angular grids in Table 1 contain 26, 110, 302, 590, and 1202 grid points. These grids have been developed by Lebedev et al.[22−24] for accurate numerical integration of spherical harmonics $Y_{l \le L,m}$ with L = 7, 17, 29, 41, and 59. It should be noted that the numbers of points in Table 1 belong to the current TURBOMOLE version.[47] For grids 3 and 5, these numbers are larger than grid sizes 3 and 5 of the first implementation (ref 28).

Our implementation of the (normalized) partition functions $P_i(\mathbf{r})$ [eq 2] follows the ideas of Becke[34] and uses the form

$$P_i(\mathbf{r}) \equiv P_i^0(\mathbf{r}) = \tilde{P}_i^0(\mathbf{r}) / \sum_{j\mathbf{L}}^{\infty} \tilde{P}_j^{\mathbf{L}}(\mathbf{r}) \quad (32)$$

with indices i and j of atoms in the reference unit cell and lattice vectors $\mathbf{L}$. The unnormalized partition functions $\tilde{P}_j^{\mathbf{L}}$ are defined as

$$\tilde{P}_j^{\mathbf{L}}(\mathbf{r}) = \prod_{k\mathbf{L}' \setminus j\mathbf{L}}^{\infty} s_{jk}^{\mathbf{L}\mathbf{L}'}(\mathbf{r}) \quad (33)$$

where indices k and $\mathbf{L}'$ run over all atoms and lattice vectors, respectively, with exception of the index pair $j\mathbf{L}$. The scaled step functions

$$s_{jk}^{\mathbf{L}\mathbf{L}'}(\mathbf{r}) = 0.5 \times [1 - h_{jk}^{\mathbf{L}\mathbf{L}'}(\mathbf{r})] \quad (34)$$

are formed using the polynomial step functions $h_{jk}^{\mathbf{L}\mathbf{L}'}$ as defined in ref 11 (cf. eq 14 in this reference), i.e.,

$$h_{jk}^{\mathbf{L}\mathbf{L}'} = \frac{1}{16} \times [35\nu_{jk}^{\mathbf{L}\mathbf{L}'} - 35(\nu_{jk}^{\mathbf{L}\mathbf{L}'})^3 + 21(\nu_{jk}^{\mathbf{L}\mathbf{L}'})^5 - 5(\nu_{jk}^{\mathbf{L}\mathbf{L}'})^7], \nu_{jk}^{\mathbf{L}\mathbf{L}'} \in [-1, 1] \quad (35)$$

with the modified confocal elliptical coordinates $\nu_{jk}^{\mathbf{L}\mathbf{L}'}$

$$\nu_{jk}^{\mathbf{L}\mathbf{L}'}(\mathbf{r}) = \mu_{jk}^{\mathbf{L}\mathbf{L}'}(\mathbf{r})/a, \quad a \in]0, 1] \quad (36)$$

The relative half-step width a is set to 0.64 as suggested in ref 11. The confocal elliptical coordinates $\mu_{jk}^{\mathbf{L}\mathbf{L}'}$ have the form

$$\mu_{jk}^{\mathbf{L}\mathbf{L}'}(\mathbf{r}) = \frac{|\mathbf{r} - \mathbf{R}_j - \mathbf{L}| - |\mathbf{r} - \mathbf{R}_k - \mathbf{L}'|}{|\mathbf{R}_j + \mathbf{L} - \mathbf{R}_k - \mathbf{L}'|} \quad (37)$$

with position vectors $\mathbf{R}_j$ and $\mathbf{R}_k$ of atoms j and k, respectively, in the reference unit cell. In cases where $\mu_{jk}^{\mathbf{L}\mathbf{L}'}$ results in $\nu_{jk}^{\mathbf{L}\mathbf{L}'} \notin [-1, 1]$, the values of the step function $h_{jk}^{\mathbf{L}\mathbf{L}'}$ are set either to 0 (for $\nu_{jk}^{\mathbf{L}\mathbf{L}'} < -1$) or to 1 (for $\nu_{jk}^{\mathbf{L}\mathbf{L}'} > 1$). For the molecular case, only the terms with $\mathbf{L} = \mathbf{L}' = 0$ remain in eqs 32−37. A fixed cutoff radius r_{cut} similar to the one suggested in ref 50 is used for the truncation of the infinite sums and products in eqs 32 and 33. If the distance between the atoms at positions $\mathbf{R}_i$ and $\mathbf{R}_j + \mathbf{L}$ is larger than r_{cut}, then the contribution $\tilde{P}_{j\mathbf{L}}$ is neglected in eq 32. Similarly, the contributions $s_{jk}^{\mathbf{L}\mathbf{L}'}$ are neglected in eq 33 for atoms at positions $\mathbf{R}_j + \mathbf{L}$ and $\mathbf{R}_k + \mathbf{L}'$ with distances larger than r_{cut}. Cutoff radii of 28 and 39 bohr are used for grids 3 and 5 and grid 7, respectively. These cutoffs yield converged values for the calculated numbers of electrons.

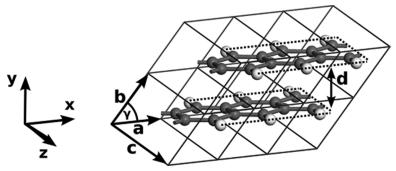

Figure 2. The 3 × 2 supercell of the aromatic chains (d = 2.451 Å). Dark and light spheres represent C and H atoms, respectively. The periodic direction of 1D and 1D (aper.) models belongs to cell parameter a. The periodic directions of 2D models correspond to cell parameters a and b.

Table 2. Dimensions m and n of $m \times n$ Supercells for Aromatic Chains[a]

model	m	n
1D	1, 2, 3, 6, 12, 23, 46, 92	1
1D (aper.)[b]	1	1, 2, 4, 8, 16, 32
2D	1, 2	1
	2, 3	2
	3, 4	3
	4	4

[a] The periodic direction of 1D and 1D (aper.) models corresponds to cell parameter a (dimension m). For 2D models, the dimensions m and n correspond to the periodic directions of cell parameters a and b, respectively. [b] See text for explanation.

The precision parameter ε [eq 20] and the threshold parameter τ [eq 27] are both set to 1×10^{-9} a.u. The program is compiled with the Portland Group Fortran 95 (PGF95) compiler version 8.0, and calculations are performed on a single x86−64 CPU (Quad-Core AMD Opteron Processor 2354, 2211.377 MHz, 512 KB cache size) under the SUSE Linux operating system using kernel version 2.6.16.

3.2. Models. The computational scaling of the algorithm is investigated using series of bulk MgO pieces, both molecular and 3D periodic, as well as 1D and 2D periodic models of aromatic chains. The MgO models are constructed from the conventional cell (lattice constant 4.211 Å, $Fm\bar{3}m$ space group) containing four MgO units and range from 1 × 1 × 1 to 5 × 5 × 5 supercells. For 1D and 2D models of aromatic chains, condensed benzene rings (bond distances b(C−C) = 1.530 Å and b(C−H) = 1.179 Å) are used. The constructed 1 × 1 UC with dimensions a = 2.65 Å, b = 3.20 Å, and γ = 50° has a C_4H_2 composition (Figure 2). Table 2 shows dimensions of the supercells used. Models denoted "1D" and "1D (aper.)" use a series of supercells increasing along the periodic direction (corresponding to a) and aperiodic direction (corresponding to b), respectively. Table 3 presents the systems used to assess the accuracy of the method. These systems range from zero dimensional (0D) molecules over periodic chains (1D) and surfaces (2D) to bulk structures (3D; see Supporting Information).

3.3. Results. Table 3 shows the relative errors of calculated electron numbers, $|\Delta N/N|$, and the exchange-correlation energies E_{XC} [eq 10]. The magnitudes of $|\Delta N/N|$ decrease from 4×10^{-6} for grid 3 to 3×10^{-8} for grid 7 and are comparable to errors obtained with previous integration schemes.[28] The exchange-correlation energies of grids 3 and 5 deviate from the E_{XC}

Table 3. Relative Errors of the Number of Electrons, $|\Delta N/N|$, and Exchange-Correlation Energies, E_{XC} (hartree)[a]

	$\lvert\Delta N/N\rvert$			ΔE_{XC}		E_{XC}
	grid					
model (periodicity)	3	5	7	3	5	7
H_2O (0D)[b]	1.3D−6	2.4D−8	4.9D−10	9.3D−6	−1.3D−7	−9.30719714
CH_4 (0D)[b]	1.3D−6	2.3D−8	7.0D−10	−1.0D−5	2.0D−7	−6.86699820
C_8H_{18} (0D)[b]	6.9D−6	1.1D−7	1.2D−8	9.8D−5	2.0D−6	−49.59078971
SiH_4 (0D)[b]	8.6D−6	3.0D−7	1.6D−8	1.5D−5	−7.4D−7	−22.36565262
SiH_4 (0D)[c]	9.4D−6	3.2D−7	1.6D−8	−4.9D−7	−3.6D−7	−22.34328264
$[C_2H_5OH]_2$ (0D)[c]	6.4D−7	5.6D−8	3.5D−10	1.7D−5	4.9D−7	−43.91399349
$[C_2H_5OH]_2$ (1D)[c]	7.2D−7	4.2D−8	2.8D−9	1.6D−5	6.3D−7	−43.90002316
$[C_2H_5OH]_2$ (2D)[c]	1.6D−6	7.4D−8	3.8D−8	2.2D−5	−3.4D−9	−43.89965668
$[C_2H_5OH]_2$ (3D)[c]	1.4D−6	5.7D−7	8.1D−8	2.5D−5	−3.0D−6	−43.89806291
$[(H_2N)_2CO]_2$ (3D)[c]	1.1D−5	2.1D−6	5.8D−8	−3.1D−5	4.1D−6	−58.58157643
$(SiO_2)_3$ (3D)[c,d]	5.6D−6	7.4D−7	5.9D−8	1.7D−4	3.4D−5	−115.00032197
$\overline{\lvert\Delta\rvert}$[e]	3.7D−6	2.1D−7	2.6D−8	3.8D−5	4.1D−6	

[a] E_{XC} of grids 3 and 5 are given by E_{XC}(grid 7) + ΔE_{XC}. [b] Calculated with TZVP basis sets. [c] Calculated with DZVP basis sets. [d] β-quartz. [e] Average of unsigned deviations

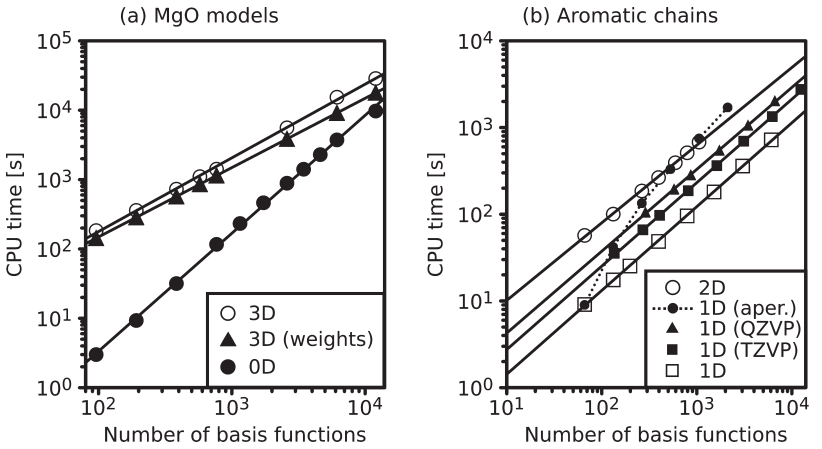

Figure 3. CPU timings of E_{XC} and matrix elements $X_{\mu\nu}^{L'}$ in one SCF step (DZVP basis sets and grid 5, if not stated otherwise).

Table 4. Scaling $O(N^x)$ of the Numerical Integration (Energy E_{XC} and Matrix $X_{\mu\nu}^{L'}$) with the System Size and Relative Errors of Electron Numbers, $|\Delta N/N|$, Using Grid 5

model	periodicity	basis	x	$\lvert\Delta N/N\rvert$
$(Mg_4O_4)_n$	0D	DZVP	1.7	4.6D−7
	3D	DZVP	1.1	6.1D−7
$(C_4H_2)_n$	1D	DZVP	1.0	2.4D−7
	1D	TZVP	1.0	3.6D−7
	1D	QZVP	0.9	2.8D−7
	1D (aper.)	DZVP	1.2[a]	3.0D−7
	2D	DZVP	0.9	1.4D−6

[a] For the supercells 1 × 8, 1 × 16, and 1 × 32.

of grid 7 in the range of 4×10^{-5} and 4×10^{-6} hartree, respectively. This demonstrates the consistent evaluation of the integrals on different grids. The use of better grids indicates the convergence of the numerically calculated values toward the exact integrals.

The CPU times required for the numerical evaluation of E_{XC} and the matrix elements $X_{\mu\nu}^{L'}$ [eq 8] are shown in Figure 3. The fitted scaling factors x summarized in Table 4 demonstrate linear scaling $O(N^{x\approx1.0})$ of our algorithm except for the series of models with increasing size in aperiodic directions, i.e., the 1D (aper.) aromatic chains and the magnesium oxide clusters. For the 1D (aper.) aromatic chains, the scaling factor x = 1.2 is obtained for larger supercells (1 × 8, 1 × 16, and 1 × 32; cf. Figure 3). For magnesium oxide clusters, linear scaling is not achieved (x = 1.7) within the investigated system sizes. In general, the size of the basis set (DZVP, TZVP, and QZVP) influences only the prefactor and not the scaling of the method.

For the bulk MgO models, the computation of the weights [eq 2] scales perfectly linearly but is almost as time-demanding as the exchange-correlation term itself (Figure 3). However, the weights have to be computed only once for a given structure, whereas the exchange-correlation term has to be computed for each SCF step. The 5 × 5 × 5 supercell of bulk MgO contains 12 000 basis functions. For this size, the computation of the weights and the exchange-correlation term requires 5 and 8 h, respectively.

Table 5. Total Number of Contributing Grid Points, n_{pt}, the Average Number of Non-Negligible Basis Functions Contributions Per Grid Point, n_{fppt}, and the Average CPU Time T (μs) for Evaluation of One Basis Function Value on a Grid Point for Selected MgO and Aromatic Chain Models (DZVP Basis Sets and Grid 5, if Not Stated Otherwise)

model	n_{pt}	n_{fppt}	T	n_{pt}	n_{fppt}	T
$(Mg_4O_4)_n$		0D			3D	
$1 \times 1 \times 1$	1.4D+5	32	0.6	1.2D+5	871	1.8
$2 \times 2 \times 2$	1.0D+6	122	0.9	9.3D+5	781	1.5
$3 \times 3 \times 3$	3.4D+6	228	1.1	3.1D+6	754	2.4
$4 \times 4 \times 4$	7.9D+6	315	1.5	7.4D+6	741	2.8
$5 \times 5 \times 5$	1.5D+7	377	1.7	1.5D+7	733	2.7
$(C_2H_4)_n$		1D			1D(QZVP)	
1×1	9.6D+4	81	1.2	9.6D+4	187	5.8
6×1	5.8D+5	75	1.1	5.8D+5	171	5.5
12×1	1.2D+6	74	1.1	1.2D+6	167	5.5
23×1	2.2D+6	74	1.1	2.2D+6	168	5.4
$(C_2H_4)_n$		1D (aper.)			2D	
1×1	9.6D+4	81	1.2	8.6D+4	294	2.3
1×4[a]	3.5D+5	204	1.8	3.4D+5	268	2.0
1×16[b]	1.4D+6	265	2.0	7.7D+5	259	2.0
1×32[c]	2.8D+6	287	2.2	1.4D+6	254	2.0

[a] Supercell for 2D: 2×2. [b] Supercell for 2D: 3×3. [c] Supercell for 2D: 4×4.

The total number of contributing grid points, n_{pt}, and the average number of non-negligible basis functions contributions per grid point, n_{fppt}, for selected MgO and aromatic chain models are shown in Table 5. These values are used to estimate the average time T for evaluation of one basis function value on a grid point (Table 5)

$$T = \frac{t_{CPU}}{n_{pt} \times n_{fppt}} \tag{38}$$

Calculations for bulk MgO and for aromatic chain models using the QZVP basis sets yield $T \approx 2$ and $T \approx 6$ μs, respectively. Therefore, the increased basis set size has a pronounced effect on T. This is because extended basis sets lead to a larger total number of non-negligible contributions. In remaining cases, the values of T are below 2 μs. The values of T facilitate future comparisons of the performance of our method with other numerical integration schemes.

4. COMPARISON WITH EXISTING METHODS

The idea of employing hierarchical structures such as the octree in integration schemes for DFT has also been explored by other authors. For example, Havu et al.[43] have investigated the application of different hierarchical structures, including the octree, in numerical integrations for both molecular and periodic systems. In their method, the levels of a tree are used to select appropriate box sizes for different spatial regions, depending on the distribution of the grid points and basis functions. However, different boxes do not overlap in space and for numerical evaluation of integrals all boxes are merged into one level. In contrast, our scheme uses boxes of different sizes at different octree levels which do overlap in space. In fact, this overlap is crucial for the efficiency of the method. To illustrate this, consider two overlapping local basis functions with very different extents, as shown in Figure 4. For each basis function, the integration boxes are larger close to their centers and decrease in size at their boundaries. Since both basis functions overlap in space the numerical integration can only be efficient if boxes of different sizes are used within the same spatial region, as in our method. If just one box is selected for each region, like in the method of Havu et al., then the size of this box may not be optimal to evaluate the contributions of both functions efficiently. In a different approach, Challacombe[14] used a tree structure to construct adaptive Cartesian grids. In contrast, our method is more general and can be applied to arbitrary integration grids and any type of local basis functions. This facilitates implementation of the method in existing DFT programs.

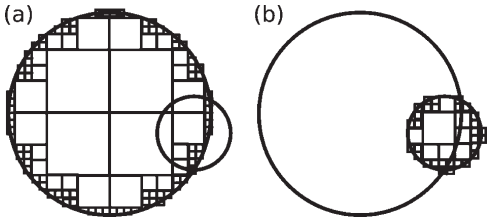

Figure 4. Schematic representation of two overlapping basis functions with different extents (shown as circles) sorted in the levels of an octree (boxes of the octree are shown as squares). The integration of the more diffuse function uses different box sizes than the integration of the compact one. This requires overlapping sets of boxes at different octree levels for the same spatial region.

5. SUMMARY

An adaptive numerical integration scheme for efficient evaluation of the exchange correlation term using localized basis functions is presented. The method treats molecular and periodic systems on an equal footing. Its computational efficiency and $O(N)$ scaling with the system size is achieved by hierarchical spatial grouping of grid points and basis functions using an octree. This grouping is used to form matrices from the values of basis functions on the grid points and allows for an optimal use of hardware-optimized matrix−matrix multiplication subroutines, such as BLAS. The novel aspect of our method is the multilevel approach using matrices of different sizes in the same region of space. This leads to the evaluation of exchange-correlation contributions with matrices of optimal sizes for basis functions of various spatial extents. The optimum choice of the matrix sizes balances the computational gain due to the efficiency of matrix−matrix multiplications and the computational loss due to negligible entries in the matrices caused by the local character of the basis functions. The implementation of the method within the TURBOMOLE program package shows linear scaling for a variety of molecular and periodic systems. The required CPU time to evaluate one basis function value on a grid point is around 2 μs for most of the systems calculated with the DZVP basis sets.

■ ASSOCIATED CONTENT

Supporting Information. Coordinates of structures listed in Table 3. This material is available free of charge via the Internet at http://pubs.acs.org.

AUTHOR INFORMATION

Corresponding Author
*E-mail: marek.sierka@chemie.hu-berlin.de.

ACKNOWLEDGMENT

This work was supported by the Deutsche Forschungsgemeinschaft (Center of Excellence UNICAT and Sonderforschungsbereich 546), the Stiftung Stipendien-Fonds des Verbandes der Chemischen Industrie, and TURBOMOLE GmbH. The authors are grateful to Professor Filipp Furche for stimulating discussions and to Professor Joachim Sauer for support.

REFERENCES

(1) Johnson, B. G.; Gill, P. M. W.; Pople, J. A. *J. Chem. Phys.* **1993**, *98*, 5612–5626.
(2) Herman, F.; Van Dyke, J. P.; Ortenburger, I. B. *Phys. Rev. Lett.* **1969**, *22*, 807–811.
(3) Perdew, J. P.; Yue, W. *Phys. Rev. B* **1986**, *33*, 8800–8802.
(4) Perdew, J. P. *Phys. Rev. B* **1986**, *33*, 8822–8824.
(5) Ghosh, S. K.; Parr, R. G. *Phys. Rev. A* **1986**, *34*, 785–791.
(6) Becke, A. D. *Phys. Rev. A* **1988**, *38*, 3098–3100.
(7) Lee, C.; Yang, W.; Parr, R. G. *Phys. Rev. B* **1988**, *37*, 785–789.
(8) Vosko, S. H.; Wilk, L.; Nusair, M. *Can. J. Phys.* **1980**, *58*, 1200–1211.
(9) Cedillo, A.; Robles, J.; Gázquez, J. L. *Phys. Rev. A* **1988**, *38*, 1697–1701.
(10) Delley, B. *J. Chem. Phys.* **1990**, *92*, 508–517.
(11) Stratmann, R. E.; Scuseria, G. E.; Frisch, M. J. *Chem. Phys. Lett.* **1996**, *257*, 213–223.
(12) Dovesi, R.; Saunders, V. R.; Roetti, R.; Orlando, R.; Zicovich-Wilson, C. M.; Pascale, F.; Civalleri, B.; Doll, K.; Harrison, N. M.; Bush, I. J.; D'Arco, P.; Llunell, M. *CRYSTAL09 User's Manual*; University of Torino: Torino, Italy, 2009.
(13) Fonseca Guerra, C.; Snijders, J. G.; te Velde, G.; Baerends, E. J. *Theor. Chem. Acc.* **1998**, *99*, 391–403.
(14) Challacombe, M. *J. Chem. Phys.* **2000**, *113*, 10037–10043.
(15) Geudtner, G.; Janetzko, F.; Köster, A. M.; Vela, A.; Calaminici, P. *J. Comput. Chem.* **2006**, *27*, 483–490.
(16) Shao, Y.; et al. *Phys. Chem. Chem. Phys.* **2006**, *8*, 3172–3191.
(17) Neese, F.; Wennmohs, F.; Hansen, A.; Becker, U. *Chem. Phys.* **2009**, *356*, 98–109.
(18) Blum, V.; Gehrke, R.; Hanke, F.; Havu, P.; Havu, V.; Ren, X.; Reuter, K.; Scheffler, M. *Comput. Phys. Commun.* **2009**, *180*, 2175–2196.
(19) Gygi, F. *Phys. Rev. B* **1993**, *48*, 11692–11700.
(20) Pérez-Jordá, J. M. *Phys. Rev. A* **1995**, *52*, 2778–2784.
(21) Rodríguez, J. I.; Thompson, D. C.; Ayers, P. W.; Köster, A. M. *J. Chem. Phys.* **2008**, *128*, 224103.
(22) Lebedev, V. I. *Siberian Math. J.* **1977**, *18*, 99–107.
(23) Delley, B. *J. Comput. Chem.* **1996**, *17*, 1152–1155.
(24) Lebedev, V. I.; Laikov, D. N. *Doklady Math.* **1999**, *59*, 477–481.
(25) Gill, P. M. W.; Johnson, B. G.; Pople, J. A. *Chem. Phys. Lett.* **1993**, *209*, 506–512.
(26) Murray, C. W.; Handy, N. C.; Laming, G. J. *Mol. Phys.* **1993**, *78*, 997–1014.
(27) Baker, J.; Andzelm, J.; Scheiner, A.; Delley, B. *J. Chem. Phys.* **1994**, *101*, 8894–8902.
(28) Treutler, O.; Ahlrichs, R. *J. Chem. Phys.* **1995**, *102*, 346–354.
(29) Mura, M. E.; Knowles, P. J. *J. Chem. Phys.* **1996**, *104*, 9848–9858.
(30) Boerrigter, P. M.; te Velde, G.; Baerends, E. J. *Int. J. Quantum Chem.* **1988**, *33*, 87–113.
(31) Averill, F. W.; Painter, G. S. *Phys. Rev. B* **1989**, *39*, 8115–8121.
(32) te Velde, G.; Baerends, E. J. *J. Comput. Phys.* **1992**, *99*, 84–98.
(33) Pederson, M. R.; Jackson, K. A. *Phys. Rev. B* **1990**, *41*, 7453–7461.
(34) Becke, A. D. *J. Chem. Phys.* **1988**, *88*, 2547–2553.
(35) Savin, A. *Int. J. Quantum Chem.* **1988**, *34* (S22), 59–69.
(36) Lin, Z.; Jaffe, J. E.; Hess, A. C. *J. Phys. Chem. A* **1999**, *103*, 2117–2127.
(37) Lindh, R.; Malmqvist, P.-Å.; Gagliardi, L. *Theor. Chem. Acc.* **2001**, *106*, 178–187.
(38) BLAS (Basic Linear Algebra Subprograms). http://www.netlib.org/blas (accessed July 25, 2011).
(39) Lawson, C. L.; Hanson, R. J.; Kincaid, D. R.; Krogh, F. T. *ACM Trans. Math. Software* **1979**, *5*, 308–323.
(40) Li, Y. S.; Wrinn, M. C.; Newsam, J. M.; Sears, M. P. *J. Comput. Chem.* **1995**, *16*, 226–234.
(41) Baker, J.; Shirel, M. *Parallel Comput.* **2000**, *26*, 1011–1024.
(42) Brown, S. T.; Kong, J. *Chem. Phys. Lett.* **2005**, *408*, 395–402.
(43) Havu, V.; Blum, V.; Havu, P.; Scheffler, M. *J. Comput. Phys.* **2009**, *228*, 8367–8379.
(44) Izmaylov, A. F.; Scuseria, G. E.; Frisch, M. J. *J. Chem. Phys.* **2006**, *125*, 104103.
(45) White, C. A.; Head-Gordon, M. *J. Chem. Phys.* **1994**, *101*, 6593–6605.
(46) White, C. A.; Johnson, B. G.; Gill, P. M. W.; Head-Gordon, M. *Chem. Phys. Lett.* **1994**, *230*, 8–16.
(47) *TURBOMOLE*, developer version; a development of the University of Karlsruhe and Forschungszentrum Karlsruhe GmbH, 1989–2007, *TURBOMOLE* GmbH, since 2007. http://www.turbomole.com (accessed Jul 25, 2011).
(48) Ahlrichs, R.; Bär, M.; Häser, M.; Horn, H.; Kölmel, C. *Chem. Phys. Lett.* **1989**, *162*, 165–169.
(49) Pople, J. A.; Gill, P. M. W.; Johnson, B. G. *Chem. Phys. Lett.* **1992**, *199*, 557–560.
(50) Towler, M. D.; Zupan, A.; Causà, M. *Comput. Phys. Commun.* **1996**, *98*, 181–205.
(51) Kudin, K. N.; Scuseria, G. E. *Phys. Rev. B* **2000**, *61*, 16440–16453.
(52) Pisani, C.; Dovesi, R.; Roetti, C. In *Hartree-Fock Ab Initio Treatment of Crystalline Systems*; Berthier, G., Dewar, M. J. S., Fischer, H., Fukui, K., Hall, G. G., Hinze, J., Jaffé, H. H., Jortner, J., Kutzelnigg, W., Ruedenberg, K., Tomasi, J., Eds.; Springer-Verlag: Berlin, 1988; Vol. 48, p 25.
(53) Sierka, M.; Hogekamp, A.; Ahlrichs, R. *J. Chem. Phys.* **2003**, *118*, 9136–9148.
(54) Schäfer, A.; Horn, H.; Ahlrichs, R. *J. Chem. Phys.* **1992**, *97*, 2571–2577.
(55) Weigend, F.; Ahlrichs, R. *Phys. Chem. Chem. Phys.* **2005**, *7*, 3297–3305.
(56) Weigend, F.; Furche, F.; Ahlrichs, R. *J. Chem. Phys.* **2003**, *119*, 12753–12762.